



**HAL**  
open science

# Seasonal and co-seismic velocity variation in the region of L'Aquila from single station 1 measurements and implications for crustal rheology 2 3 AUTHORS

Piero Poli, Valenting Marguin, Qingyu Wang, Nicola d'Agostino, Paul A. Johnson

## ► To cite this version:

Piero Poli, Valenting Marguin, Qingyu Wang, Nicola d'Agostino, Paul A. Johnson. Seasonal and co-seismic velocity variation in the region of L'Aquila from single station 1 measurements and implications for crustal rheology 2 3 AUTHORS. *Journal of Geophysical Research: Solid Earth*, 2020, 125 (7), pp.e2019JB019316. 10.1029/2019JB019316 . hal-02929924

**HAL Id: hal-02929924**

<https://hal.univ-grenoble-alpes.fr/hal-02929924v1>

Submitted on 4 Sep 2020

**HAL** is a multi-disciplinary open access archive for the deposit and dissemination of scientific research documents, whether they are published or not. The documents may come from teaching and research institutions in France or abroad, or from public or private research centers.

L'archive ouverte pluridisciplinaire **HAL**, est destinée au dépôt et à la diffusion de documents scientifiques de niveau recherche, publiés ou non, émanant des établissements d'enseignement et de recherche français ou étrangers, des laboratoires publics ou privés.

1 ***Seasonal and co-seismic velocity variation in the region of L'Aquila from single station***  
2 ***measurements and implications for crustal rheology***  
3

4 **AUTHORS:** *Piero Poli<sup>1</sup>, Valenting Marguin<sup>2</sup>, Qingyu Wang<sup>1</sup>, Nicola D'Agostino<sup>3</sup>, Paul*  
5 *Johnson<sup>4</sup>*  
6

7 1- *Institut de Sciences de la Terre, Université Grenoble Alpes, CNRS (UMR5275),*  
8 *Grenoble, France.*

9 2- *Département des sciences de la Terre, Université de Genève, 1205 Geneva,*  
10 *Switzerland*

11 3- *Osservatorio Nazionale Terremoti, Istituto Nazionale Geofisica Vulcanologia, Roma,*  
12 *Italy*

13 4- *Geophysics, Los Alamos National Laboratory, Los Alamos, New Mexico USA 87545*  
14

15 ***ABSTRACT***

16 *We performed time lapse measurements of velocity variations using empirical Green's*  
17 *functions reconstructed by autocorrelation of seismic noise recorded during a period of 17*  
18 *years in the region of l'Aquila, Italy. The time lapse approach permitted us to evaluate the*  
19 *spatial (depth) dependence of velocity variation (dv/v). By quantitatively comparing the 17*  
20 *years of dv/v time series with independent data (e.g. strain induced by earthquakes,*  
21 *hydrological loading) we unravel a group of physical processes inducing velocity variations*  
22 *in the crust over multiple time and spatial scales. We find that rapid shaking due to three*  
23 *magnitude 6+ earthquakes mainly induced near surface velocity variations. On the other hand,*  
24 *Slow strain perturbation (period 5 years) associated with hydrological cycles, induced velocity*  
25 *changes primarily in the middle-crust. The observed behavior suggests the existence of a large*  
26 *volume of fluid filled cracks exist deep in the crust. Our study, beyond shedding new light into*  
27 *the depth dependent rheology of crustal rocks in the region or l'Aquila, highlights the*  
28 *possibility of using seasonal and multiyear perturbations to probe the physical properties of*  
29 *seismogenic fault volumes.*  
30

31 ***1. Introduction***

32 Detailed laboratory protocols exist to estimate how rocks respond to strain  
33 perturbations, and show that a variety of non-linear responses exists for variable rock types  
34 with different physical properties (e.g. cracks density, microstructure, presence of fluid,  
35 temperature and pressure effects—Guyet & Johnson, 1999;2009; Ostrovsky and Johnson,  
36 2001; Renaud et al., 2009, 2012, Riviere et al., 2015).

37 One approach to describing nonlinear elastic and plastic properties of rock is applying  
38 'effective viscosity' (e.g. Lyakhovskiy et al., 2001, Ben-Zion, 2008). Numerical simulations  
39 (Lyakhovskiy et al., 2001, Hamiel et al., 2006; Lott et al.2018) show how this effective  
40 parameter plays a fundamental role in how rocks respond to strain perturbation, and thus  
41 controls phenomena occurring during the seismic cycle (e.g. clustering of seismicity,  
42 foreshocks, style of nucleation, amount of aseismic slip). The effective viscosity parameter  
43 has similarities to the hysteretic nonlinear parameter in the Priesach-Mayergoyz description  
44 of elasticity (McCall and Guyet 1993; Guyet and Johnson 2009). The latter has a direct  
45 link with damage intensity (e.g., Guyet and Johnson 1999; Johnson 1998, Van Den Abeele  
46 and Visscher, 2000, Ostrovsky and Johnson 2001). Other models that describe these  
47 behaviours, as well including Arrhenius approaches for hysteresis, exists (e.g., Ostrovsky  
48 et al., 2019; Sens-Schoenfelder et al., 2018).

49 It is thus fundamental to characterize the physical properties of rocks surrounding  
50 seismogenic faults, to better understand the role of rheology and elasticity during the

51 seismic cycle, and associated phenomena that can arise in fault(s). Field observations  
52 emulating laboratory protocols have been attempted, by studying velocity variations due to  
53 strong, surface active-source induced shaking (e.g., Johnson et al., 2009), as well as rocks  
54 subjected to cycles of tidal forcing and induced seismicity (e.g., Deloey et al, 2017; van  
55 der Elst et al, 2017 and active seismic experiments probing the effects of Earth tides (e.g.  
56 Yamaura et al., 2003). More recently, the ability of estimating the Green's function from  
57 seismic noise (Shapiro & Campillo, 2004), has made it possible to monitor velocity  
58 variations (e.g. Brenguier et al., 2014) without the need of active sources (e.g. explosions;  
59 vibrators), and more recent studies applied this method to study the response of rocks to  
60 tidal strain (Takano et al., 2014, Hillers et al., 2015b). However, at present only the  
61 shallowest portions of the crust (primarily less than 1km of depth) have been explored  
62 (Takano et al., 2014, Hillers et al., 2015b) and at most, depths to 5 km, following the 2004  
63 M6.0 Parkfield earthquake (Wu et al., 2017), thus permitting the characterization of  
64 shallow damage zones, but not deeper regions, where the most seismicity occurs and large  
65 earthquakes nucleate (see Ben-Zion, 2008, and reference therein).

66 It has been demonstrated that detailed lapse-time monitoring applying coda waves  
67 reconstructed from correlation of seismic noise can provide important information about  
68 the deeper part of the crust (Obermann et al., 2013, Obermann et al., 2014, Hillers et al.,  
69 2018). These results have been validated with numerical experiments, providing clues  
70 regarding the depth resolution of velocity variation ( $dv/v$ ) as function of coda lapse-time  
71 (Obermann et al., 2013).

72 In this work, we performed time lapse monitoring of  $dv/v$  near to the city of L'Aquila,  
73 in the central Apennines (Italy). This region is characterized by active normal faulting that  
74 accommodates the ongoing  $\sim 3$  mm/yr tectonic extension (D'Agostino, 2014, Fig. 1). As a  
75 result, normal faults capable of producing magnitude 6+ events are present along the entire  
76 Apennine chain. The region of L'Aquila itself is characterized by significant seismic  
77 hazard, and was recently struck by 3 magnitude 6+ earthquakes (<http://iside.rm.ingv.it>, Fig.  
78 1).

79 We here estimate the spatial (depth) response ( $dv/v$ ) of the medium to periodic  
80 perturbations. Instead of relying of tidal strain as has been applied by others (e.g., Hillers  
81 et al., 2015), we exploit periodic perturbations associated with multiyear-long hydrological  
82 cycle related to the recharge of karst aquifers (e.g. Silverii et al., 2019). These perturbations  
83 provide significant strain at the surface (relative baseline elongation up to 10-6 mm within  
84 few tens of kilometers, mostly horizontal) with poorly resolved extension at depth.  
85 Correlation with seismicity rate in the 1.2-3.9 magnitude range in the southern Apennines  
86 (D'Agostino et al., 2019) suggests that stress perturbations induced by the hydrological  
87 forcing may extend to a depth larger than 5 km and thus affect the seismogenic portion of  
88 the crust (Fig. 1). In particular, we assess how  $dv/v$  over different time windows, evolves  
89 for episodes of dilatation and compression of the crust (Silverii et al., 2019). We further  
90 estimate the response of the medium to earthquakes ( $M > 6$ ) that occurred during the study  
91 period (2000-2016).

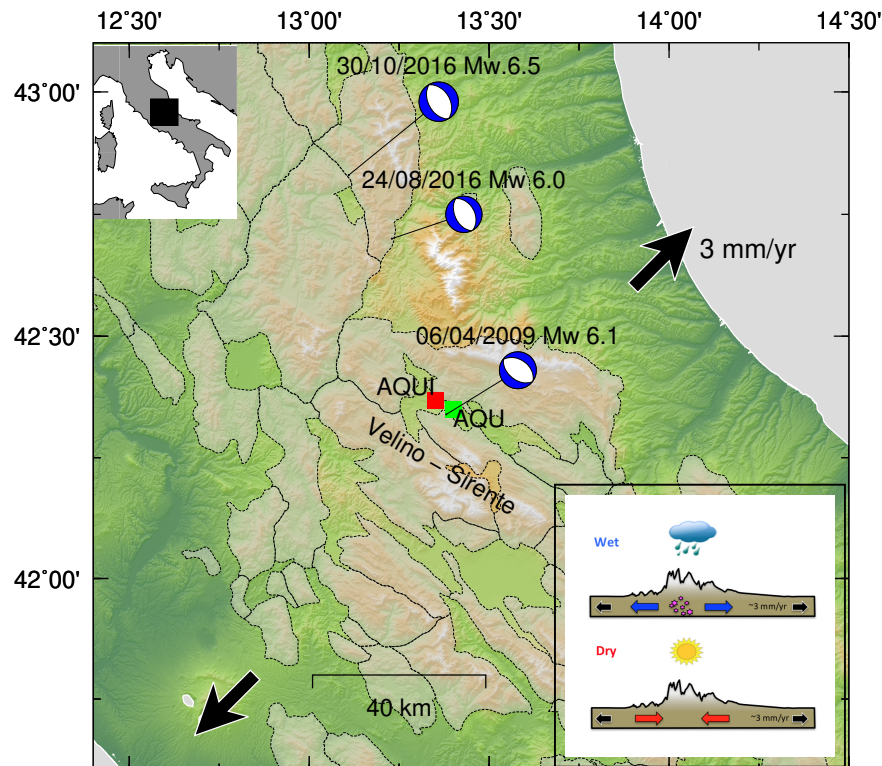
92 In the following, we begin by describing the procedures to derive estimates of the  
93 Green's function and measure velocity variations (sec. 2). We then analyze evolution of  
94  $dv/v$  for periodic perturbation and during coseismic periods (sec. 3 and 4). Finally, we  
95 discuss the results and the peculiar evolution of  $dv/v$  as a function of lapse-time that we  
96 observed (sec. 5). Our results suggest that an isolated region extended into the middle-  
97 lower crust is particularly sensitive to deformations. We interpret this observation as due  
98 to the presence of significant amounts of fluid filled cracks at depth that make the material  
99 more susceptible to the nonlinear elastic changes we observe.

101 **2. Seismic noise correlation and time lapse velocity variation**

102  
103 **a. Estimation of the Green's function from noise correlation**

104 We calculate the three-component (ZZ, EE, NN) autocorrelation using continuous  
105 seismic data recorded at the AQU station located in central Italy (Fig. 1). We focus on the  
106 time period from January 1 2000 to December 31 2017 (17 years). Each daily trace of  
107 seismic data is split in 10min windows with 50% overlap, after the deconvolution of the  
108 instrumental response and filtering between 0.5 and 1Hz. After analyzing several frequency  
109 bands, we choose to focus on 0.5-1Hz range as it provides the highest quality correlation,  
110 while limiting the amount of stacked days, thus increasing the time resolution of our  
111 analysis.

112 To remove spurious spikes and contributions from earthquakes, we calculate the sum  
113 of the squared signal (energy) for each window, and remove those exceeding the daily mean  
114 of the energy plus 3 standard deviations (Poli et al., 2012). We ensure that, after this test,  
115 at least 20 hours of data are still contained in the daily trace; otherwise the daily trace is  
116 rejected. The time windows passing the amplitude test are one-bit normalized to further  
117 reduce transient signals (e.g. earthquakes), which may escape our processing.  
118  
119



120  
121  
122  
123 **Figure 1.** Map of the study area. The upper inset shows the location of the study  
124 area in Italy. The squares indicate the location of the seismic (AQU, in green) and GPS  
125 (AQU1, in red) stations. Beach balls show focal mechanism of the main events from 2009  
126 to 2016 (from Scognamiglio et al., 2006). Shaded areas include regions where carbonate  
127 lithologies host large karst aquifers (see Silverii et al., 2019). The lower inset shows a  
128 conceptual drawing of the modulation of crustal deformation and seismicity by seasonal  
129 and multi-annual recharge/discharge phases of of karst aquifers.  
130



131  
132  
133  
134  
135  
136  
137  
138  
139  
140  
141  
142  
143  
144  
145  
146  
147  
148  
149  
150  
151  
152  
153  
154  
155  
156  
157  
158  
159  
160  
161  
162  
163  
164  
165  
166  
167  
168  
169  
170  
171  
172  
173  
174  
175  
176  
177  
178  
179  
180

***b. Measurement of velocity variation ( $dv/v$ )***

We measure the velocity variations using both stretching (Lobkis & Weaver, 2003) and doublet (Poupinet et al., 1984) techniques. While the two methods provide similar results (Fig. S3), additional tests have shown that the stretching technique provides less noisy measurements, and therefore will be used here.

In detail, the velocities are obtained by stacking 90 days using a 89 day overlap of correlations, to ensure stable  $dv/v$  measures (Sabra et al., 2005). Each stacked correlation is then compared, using the methods mentioned above, with a reference signal (the stack of the correlation over the full-time period) to estimate the  $dv/v$  over different coda waves lapse-time (table 1). We then average the  $dv/v$  over different components, weighting with squared correlation coefficients estimated after stretching. Only signals with correlation larger than 0.9 are retained, and a stack is performed if all the 3 components are available.

***c. Lapse time and depth sensitivity of  $dv/v$***

In this section, we estimate the first order depth resolution for our velocity variation measures. It should be kept in mind however, that the sensitivity to absolute depth requires detailed measures of the scattering properties of the medium, which are not available for the study area (Obermann et al. 2013; 2016, Kanu and Snieder, 2015). Nevertheless, we can reason around existing theoretical and numerical results to gain insights about relative depth resolution of coda waves measured at different lapse time of the coda (Obermann et al. 2013; 2016, Kanu and Snieder, 2015).

Despite the depth sensitivity of coda waves has not been fully quantitatively solved yet, it is well known that the sensitivity to  $dv/v$  in a medium varies with frequency and time lapse of the coda waves used (i.e., deeper sampling for larger lapse-time) (e.g. Pacheco & Snieder, 2005, Obermann et al., 2013, Wu et al., 2017). Numerical simulations (Obermann et al. 2013, 2016) reported that the sensitivity of coda waves is due to a combination of the sensitivities of body waves and surfaces waves. In the early normalized lapse-time,  $t$  less than  $\sim 6$  ( $t$  is normalized by mean free time  $t^*$ ), the coda wave sensitivity is controlled by the surface wave sensitivity. With increasing lapse-time, the body wave sensitivity becomes progressively more important.

We thus start by estimating the sensitivity of surface waves (Hermann, 2013), using a local velocity model (Chiaraluce et al., 2009) and a frequency of 0.75Hz (Fig. 2b). The resulting surface wave kernel suggest sensitivity in the uppermost 4km of the crust.

We furthermore evaluate the sensitivity of the scattered body waves by considering a 3-D sensitivity kernel formulation by Pacheco and Snieder (2005). The energy propagator  $p$  is calculated by the radiative transfer solution approximation for isotropic scattering (Paasschens, 1997; Planès et al., 2014). We estimate the theoretical depth sensitivities of the body wave velocity changes with scattering mean free paths from 10 km and 100 km, proxies for the high and low frequency regimes (Lacombe et al., 2003, Hiller et al., 2019). The energy velocity is determined by the equipartition state. We take the theoretical equipartition ratio as 10.4 and 3 for a Poisson solid (Margerin et al., 2000; Weaver, 1982), the same as Wang et al. (2019), for further calculation. We solved for the body wave depth sensitivity normalized to 30 km depth with each layer 1 km thick layer.

Figure 2a gives the calculated normalized body wave kernel. The calculation follows the details described by Obermann et al., (2013), Planès et al. (2014), Obermann et al. (2016), and Wang et al., (2019). We clearly observe that using the mean free path ( $l$ ) equal to 100 km (low frequency regime), the depth sensitivity is deeper than using the smaller mean free path  $l$  as 10 km. This is an indication of the frequency-dependent depth

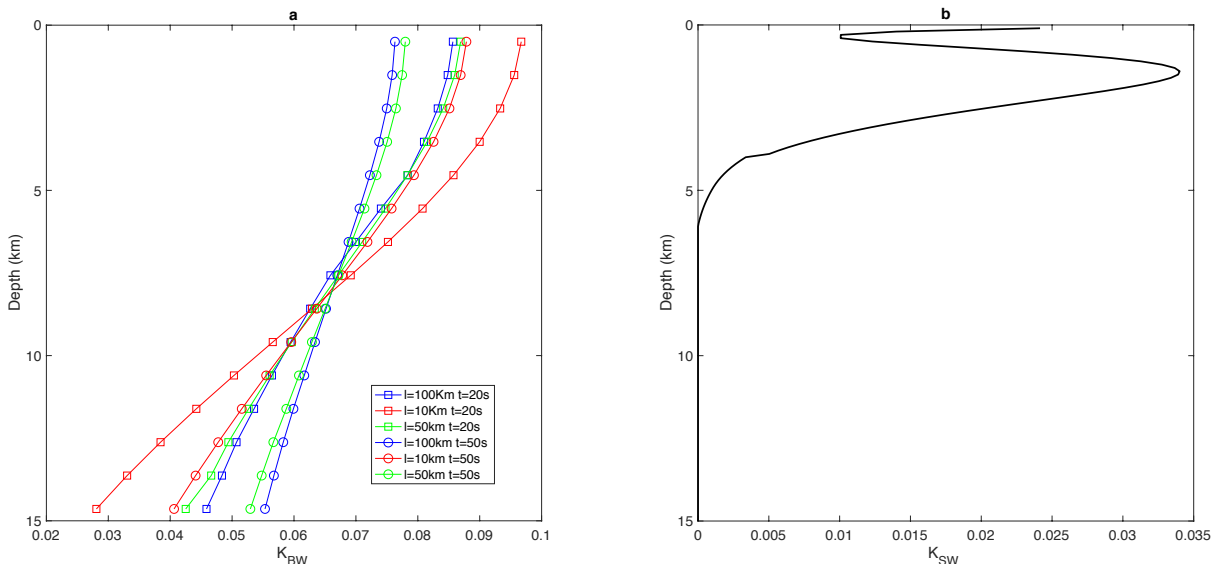
181 sensitivity of body waves, which is the same characteristic surface waves exhibit (Fig. 2a).  
 182 We also observe how the depth sensitivity increases gradually as the lapse-time becomes  
 183 progressively larger from 20 s to 50 s with the same mean free path. Thus, we measure the  
 184 seismic velocity changes for deeper strata applying later lapse-times (Fig. 2a). This result,  
 185 suggest that by observing the time-lapse evolution of  $dv/v$  across the coda, we can get  
 186 insights about velocity variation into deep layers. A similar conclusion was draw by  
 187 Obermann et al. (2013) by using numerical modeling.

188 Guided by the calculated kernels and results from previous studies (Obermann et al.  
 189 2013), we defined a set of windows (table 1) to scan different depths of the crust, similarly  
 190 to previous studies based on autocorrelation (e.g. Richter et al., 2014). In more detail, we  
 191 defined 3 starting times (10, 20, and 30s) after zero time (ballistic waves arrival time). For  
 192 each starting time, we vary the length of the time window to perform stretching (20, 40,  
 193 60s). The goal of this coda lapse-time dependent analysis is to resolve any evolution of  
 194  $dv/v$ , which can reveal the linear and nonlinear elastic response as function of relative depth  
 195 (e.g. increment of  $dv/v$  with coda lapse time will highlight larger velocity changes at depth).  
 196

197 **Table 1:** Time lapse for calculation of  $dv/v$ .

<i>Window number</i>	<i>Time start (s)</i>	<i>Time end (s)</i>
<b>1</b>	10	30
<b>2</b>	10	50
<b>3</b>	10	70
<b>4</b>	20	40
<b>5</b>	20	60
<b>6</b>	20	80
<b>7</b>	30	50
<b>8</b>	30	70
<b>9</b>	30	90

198  
 199



200 **Figure 2:** a) Body waves sensitivity kernels for variable mean free paths lapse-times.  
 201 b) Surface waves sensitivity kernel.

202  
 203  
 204 **d. Comparison of  $dv/v$  with other estimates**

205 The velocity variation ( $dv/v$ ) time series for window 4 (20s to 40s lag time) is shown  
206 in figure 3 (measures for the other time lapse intervals are shown in figures 4 and 7, for  
207 periodic and co-seismic perturbations respectively). Two primary velocity decreases are  
208 observed. The largest decrease (relative  $dv/v \sim 0.3\%$ ) is associated with the occurrence of  
209 the magnitude 6.3 L'Aquila earthquake ([iside.rm.ingv.it](http://iside.rm.ingv.it)). The second decrease (relative  
210  $dv/v \sim 0.15\%$ ) occurred in 2016 during the Norcia-Visso seismic sequence (Chiaraluce et  
211 al., 2016), which includes 2 M6+ earthquakes. Besides of these major coseismic drops, we  
212 observe cyclic variations of  $dv/v$  up to 0.05% (fig. 3b).

213 Silverii et al. (2016, 2019) analyzed GPS data in the study region, showing the presence  
214 of transient deformations associated with multiyear hydrological cycles ( $\sim 5$  yrs). During  
215 these cycles the crust undergoes significant extension and compression (up to 3mm/yr)  
216 sustained for 2-3 years associated, respectively, with phases of recharge and discharge of  
217 karst aquifers that modulate the secular, tectonic strain accumulation (see inset Fig. 1).  
218 These cycles are visible in both the rain time series (shown as detrended cumulative rain in  
219 fig. 3c) and in the detrended horizontal GPS motion (fig. 3e) recorded at the station AQUI  
220 (fig. 1). Here we use the east-component time series of the AQUI site corrected for long-  
221 term trend and instrumental offsets (see Silverii et al., 2019 for details of the processing).

222 In periods of significant aquifer recharge (e.g. 2005 to 2007) the AQUI site is subject  
223 to a significant eastward displacement ( $\sim 5$ mm), while the opposite motion is recorded for  
224 dry periods. As reported by Silverii et al (2019) the multi-seasonal, hydrological forcing  
225 associated to the recharge of karst aquifers induces a measurable surface deformation up to  
226  $\sim 90$  nanostrain/yr. The AQUI station is mostly sensitive to the large Velino-Sirente karst  
227 system (Fig. 1) alternatively moving to the north-east during phases of high recharge and  
228 to the south-west during phases of low-recharge (Silverii et al., 2019). This motion is  
229 superimposed on the steady SW-NE 3 mm/yr extension across the Apennines. It is  
230 important to note that this phenomenon is pervasively observed along the Apennines at  
231 stations located close to main karst aquifers (Silverii et al., 2016, 2019; D'Agostino et al.,  
232 2018).

233 Similarly, and in agreement with previous studies (e.g. Hillers et al., 2015a, Wang et  
234 al. 2017), the  $dv/v$  follows the hydrological cycle, with a velocity drop for increasing  
235 hydraulic head and vice versa. The  $dv/v$  also shows shorter term oscillations ( $\sim 1$ yr) which  
236 are visually correlated with the variation of surface temperature (fig. 3d). In agreement with  
237 previous studies (e.g. Richter et al., 2014) a decrease in temperature coincides with a  
238 reduction of  $dv/v$ . Alternatively, these, short-term oscillations can be due to short term  
239 seasonal hydrological effects similar to what is observed in the GPS time series (Silverii et  
240 al., 2016).

241 In the remainder of this work we will quantify the response of the crust to periodic  
242 (hydrological) and tectonic (earthquakes) forcing and assess the sensitivity of different  
243 crustal levels to these deformations.

244  
245

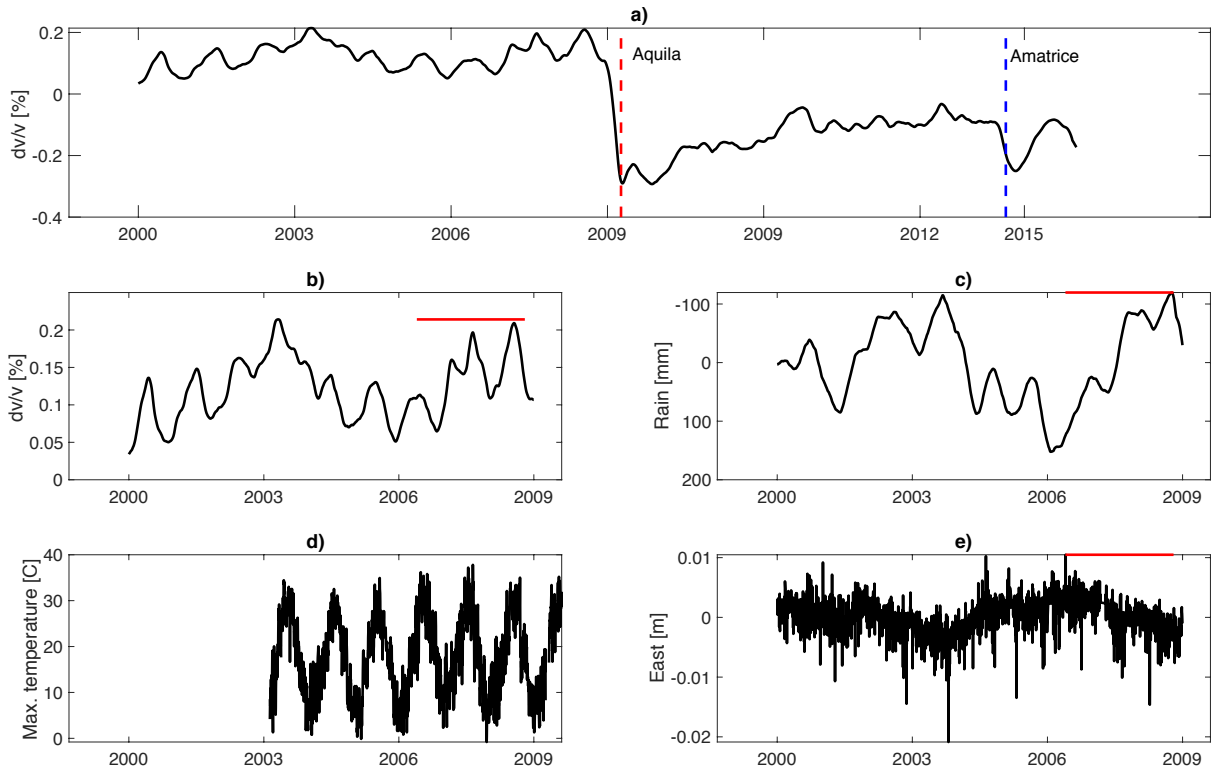


**FIGURE 3:** Summary of observations in the study area. a) Time series of velocity variation for the entire period, with major earthquakes highlighted. b)  $dv/v$  time series during the preseismic period. c) Detrended cumulative rain as in Silverii et al. (2019) ( $y$ -axis is inverted). d) Daily maximum temperature. e) East GPS displacement at station AQUI corrected for tectonic trend and antenna offset from Silverii et al. (2009). The red solid line indicate a dry period identified by Silverii et al. (2009).

### 3. Sensitivity to cyclic deformations and probing the mid-crust

#### a. Decomposition of $dv/v$ time series

We quantitatively evaluate the seasonal and multi-years components of  $dv/v$  estimated for different lapse times (see table 1). In this section, we focus only on the pre-seismic period, using  $dv/v$  measured before L'Aquila earthquake (beginning of 2000 to end of 2008).

We start by modeling the relative contribution of the multiyear and seasonal effect on  $dv/v$  with a phenomenological model (e.g. Taira et al, 2018):

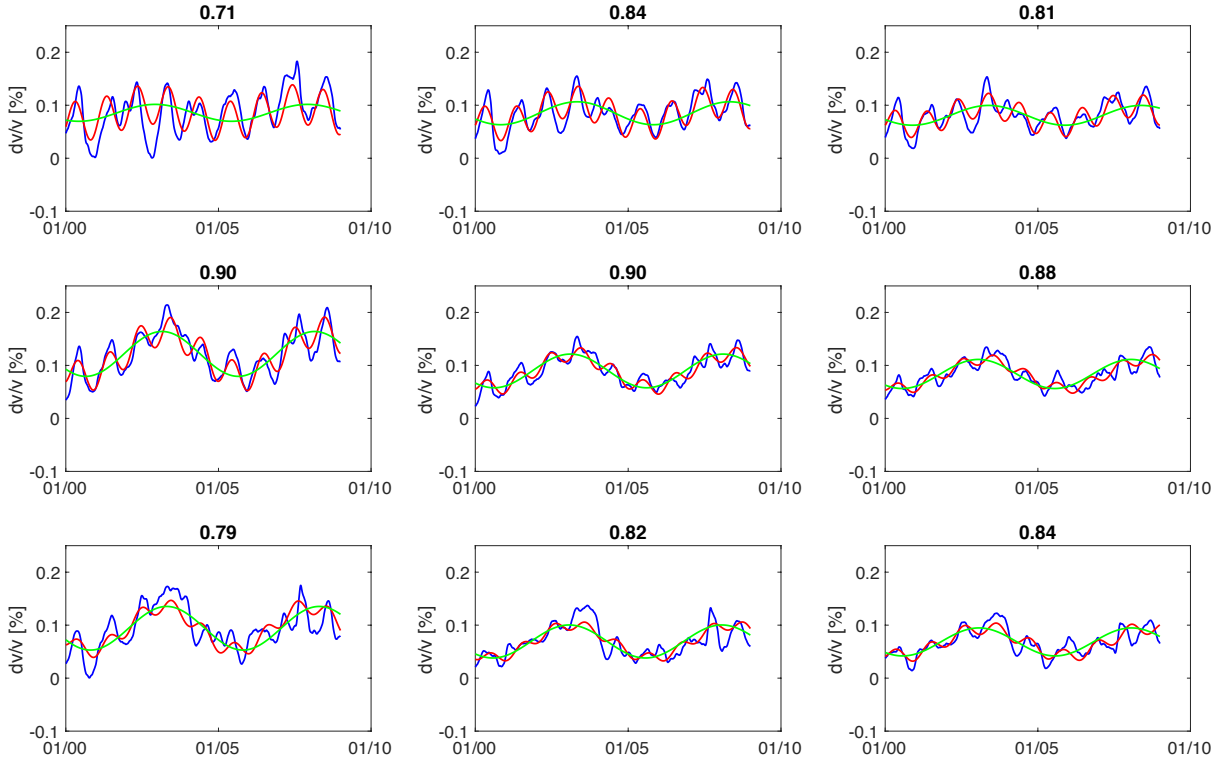
$$\frac{dv}{v_S} = A + B \cos\left(\frac{2\pi}{C \cdot 365}(t - D)\right) + E \cos\left(\frac{2\pi}{F \cdot 365}(t - G)\right) \quad [2]$$

In eq. 2,  $A$  is a global offset,  $B$  and  $E$  are the amplitudes of the two modelled cycles,  $C$  and  $F$  are the cycle duration in years, while  $D$  and  $G$  account for the cosine phase shift. We fit all  $dv/v$  time series using a non-linear least squares approach. From the inversion, we find that for all selected time lapses the best-fit durations of the cycles are  $C=1 \pm 0.02$ yr and  $F=5 \pm 0.1$  yrs.

The results of our fits are shown in figure 4 (red and green lines) together with the original data (blue lines). It can be observed that while the  $dv/v$  amplitude of seasonal 1-yr oscillation ( $B$ ) is higher at earlier lapse times, progressive decreases in the later coda are observed where  $dv/v$  is more sensitive to the 5yr cycle ( $E$ ). To better

276  
277  
278  
279  
280  
281

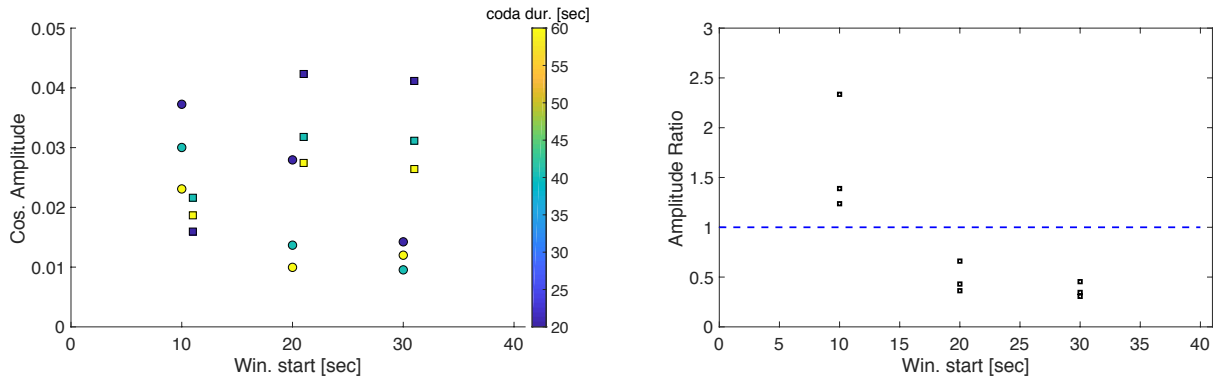
visualize the results, we plot in figure 5 the B and E terms of equation 2 as function of coda lapse time. While the amplitude of the short-term cycle decreases at larger lapse time, the opposite behavior is observed for the amplitude of the 5-yrs (E). The ratio of the B and E parameters (fig. 5b) suggests that beyond 20s lapse time  $dv/v$  is dominated by the long-term cycle.



282  
283  
284  
285  
286  
287  
288  
289  
290  
291  
292  
293  
294  
295  
296  
297

**Figure 4:**  $dv/v$  (blue) and modeled cycles with eq. 2 (red) for coda windows reported in table 1. The green line represents the long-term portion (first and third righthand terms of eq. 1). Numbers on top of each plot are the correlation coefficient between the model (eq. 2, red) and the data (blue).

The decay of the parameter B (fig. 3a) and the B/E ratio (fig. 3b), suggests that the source of the 1yr periodicity in  $dv/v$  is dominantly at shallow depths (Obermann et al., 2013, see also the kernels in fig. 2). It has been suggested that thermally induced stresses rapidly decays with depth (Ben-Zion & Leary, 1986), and the effects on  $dv/v$  have been reported in other regions (e.g. Richter et al, 2014). Thus, as the short-term cycle closely follows the seasonal temperature variation (fig. 3d, see fig S1) and shows a rapid decay as a function of depth, we infer that temperature plays a primary role in controlling the  $dv/v$ .



298  
 299 **Figure 5:** Magnitude of  $B$  (round) and  $E$  (squares) as function of coda window time  
 300 (left). The color indicates the duration of the window. Squares are offset by 1sec for  
 301 clarity. Ratio  $B/E$  as function of coda window order (right, black).  
 302

303 The long period oscillations of  $dv/v$  are strongly correlated with the long-term  
 304 variation of rainfall (fig. 3c) and GPS deformation (fig. 3e, S2). This multiyear signal  
 305 represents transient deformations, occurring in highly fractured crustal rock as a  
 306 response to variations of the hydraulic head in karst aquifers, and induces a strain rate  
 307 up to  $\sim 90$  nanostrain/yr (Silverii et al., 2019). This strain rate temporarily increases  
 308 during high recharge, or diminishes during droughts, and can locally exceed the long-  
 309 term secular tectonic strain rate (D’Agostino, 2014). The  $dv/v$  for later lapse times  
 310 better correlates with this long period deformation (fig. 5). This observation suggests  
 311 that a particular depth of the crust is more susceptible to these periodic perturbations  
 312 (Obermann et al., 2013). Furthermore, we observe how for these late lapse-times (or  
 313 depths) the short-term cycle has limited effect (2 to 4 times smaller, Fig. 5). As the  
 314 thermally induced stress rapidly decays with depth (Ben-Zion & Leary, 1986), we can  
 315 further confirm that the late coda evolution of  $dv/v$  is sensitive to deeper layers.  
 316

### 317 ***b. Probing the crust with long term (5yrs) periodic deformations***

318 We probe the rheological response of the crust to these perturbations using time  
 319 lapse measures of  $dv/v$ , similar to what has been done in other regions with tidal strain  
 320 (Takano et al., 2014, Hillers et al., 2015b). To reiterate, the goal is to derive a lapse  
 321 time (or depth) dependent measurements of  $dv/v$  representative of perturbations at  
 322 different crustal levels in order to reveal physical properties of rocks at different depth  
 323 (e.g. Obermann et al., 2015, Hillers et al., 2018).

324 The *in-situ* measurements resemble laboratory dynamic acoustoelastic testing,  
 325 a ‘pump-probe’ method (e.g., Renaud et al., 2009, 2012). Here, the medium changes  
 326 are evaluated by estimating  $dv/v$  using the reconstructed Green’s function (the ‘probe’),  
 327 while the medium is deformed by long period ( $\sim 5$  yrs) perturbations (the ‘pump’) shown  
 328 by the GPS signal (Silverii et al., 2019, Fig. 2). More precisely, we create a new set of  
 329 autocorrelations by stacking 300 days of data with 200 days overlap. This time  
 330 windowing helps us to reduce the short-term fluctuations (1yr). For each time segment  
 331  $dv/v$  is estimated by comparing the estimated Green’s function, with a reference signal  
 332 from stacking over the full period (2000 to end of 2008). We use the stretching method  
 333 and the same coda time windows listed in table 1. The deformation is obtained from  
 334 the projection of the east and north components of the GPS time series recorded at the  
 335 AQUI station (Fig. 1), along the N45 direction, to maximize the amplitude of the  
 336 hydrologically-related deformation ( $\hat{d}$ ) (Silverii et al., 2019). The GPS time series is  
 337 indicative for the strain in the crust (Silverii et al., 2019): negative (south-westward)  $\hat{d}$



338 correspond to horizontal contraction, whereas positive  $\hat{d}$  (north-eastward) values are  
339 representative of horizontal dilatation.

340 We then infer the sensitivity of  $dv/v$  to deformation in each time window by  
341 fitting the data (fig. 6) with a linear model:

$$\frac{\delta v}{v} = \alpha + \beta \hat{d} \quad [3]$$

342  
343  
344  
345 Equation 3 is similar to strain- $dv/v$  relationship used to study the sensitivity to  
346 tidal strain (Takano et al., 2014, Hillers et al., 2015b), where  $\beta$  represents the sensitivity  
347 to deformation while the zero-offset is  $\alpha$ . Our phenomenological model can be  
348 compared to the 1-D non-linear elasticity equation derived in Landau and Lifshutz  
349 (2012) and broadly applied to Earth materials (e.g., Guyer and Johnson, 1999;2009).  
350 We can interpret the sensitivity to elastic deformation ( $\beta$ ) as the classic non-linear  
351 elastic parameter that describes the slope of  $\delta v/v$  over a single low frequency pump  
352 cycle.  $\alpha$  is the non-linear volumetric change (length change in 1D) related to material  
353 conditioning (Guyer & Johnson, 2009). Note in eq. 3 we do not include the cubic non-  
354 linear elastic parameter that describes curvature in  $\delta v/v$  as the scattering in the data  
355 provide similar misfit for 1<sup>st</sup> and 2<sup>nd</sup> order polynomial fit, nor the hysteretic term that is  
356 common to Earth materials.

357 The results in figure 6 show that, in agreement with experimental observations  
358 in laboratory rock samples (e.g. Renaud et al., 2012), velocity increases under  
359 compression (negative  $\hat{d}$ ) and reduces during expansion episodes (positive  $\hat{d}$ ). Similar  
360 results have been obtained by analyzing the relation between  $dv/v$  and tidal strain using  
361 active source data (Yamamura et al., 2003) or noise correlation (Takano et al., 2014).  
362 A similar response to crustal dilatation has also been observed during tectonic transient  
363 deformation (Rivet et al., 2011). We also note that the parameter  $\beta$  decreases with  
364 increasing lapse time (fig. 6). This lapse time evolution, combined with the depth  
365 kernels (fig. 2), suggests that the long-period strain perturbations sample primarily at  
366 depth (Obermann et al., 2015), rather than close to the free surface.

367 Before entering in the interpretation of this result, we will estimate the  
368 sensitivity to co-seismic strain perturbation (sec. 4).

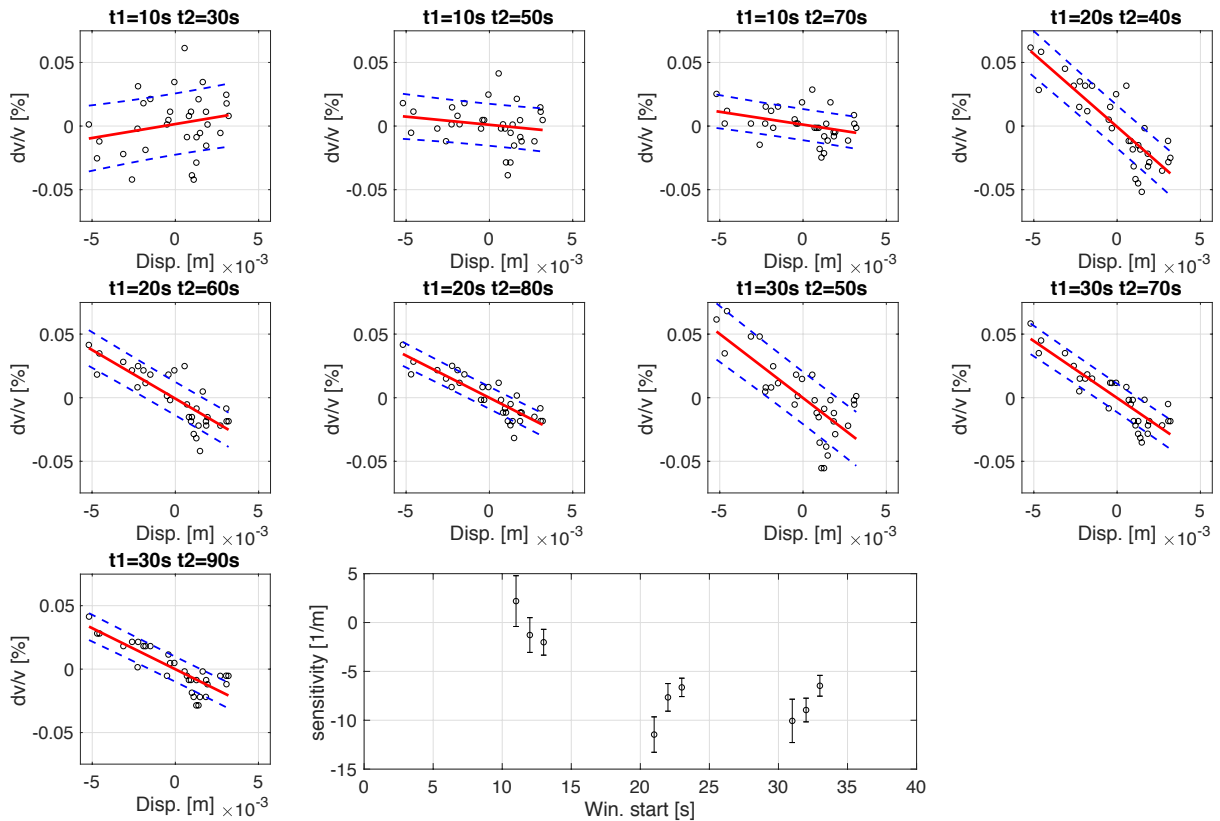


**Figure 6:** The scatter plot represents the fit of displacement and  $dv/v$  using equation 3. The last plot is the parameter  $\beta$  of equation 3 as function of coda lapse time (Table 1).

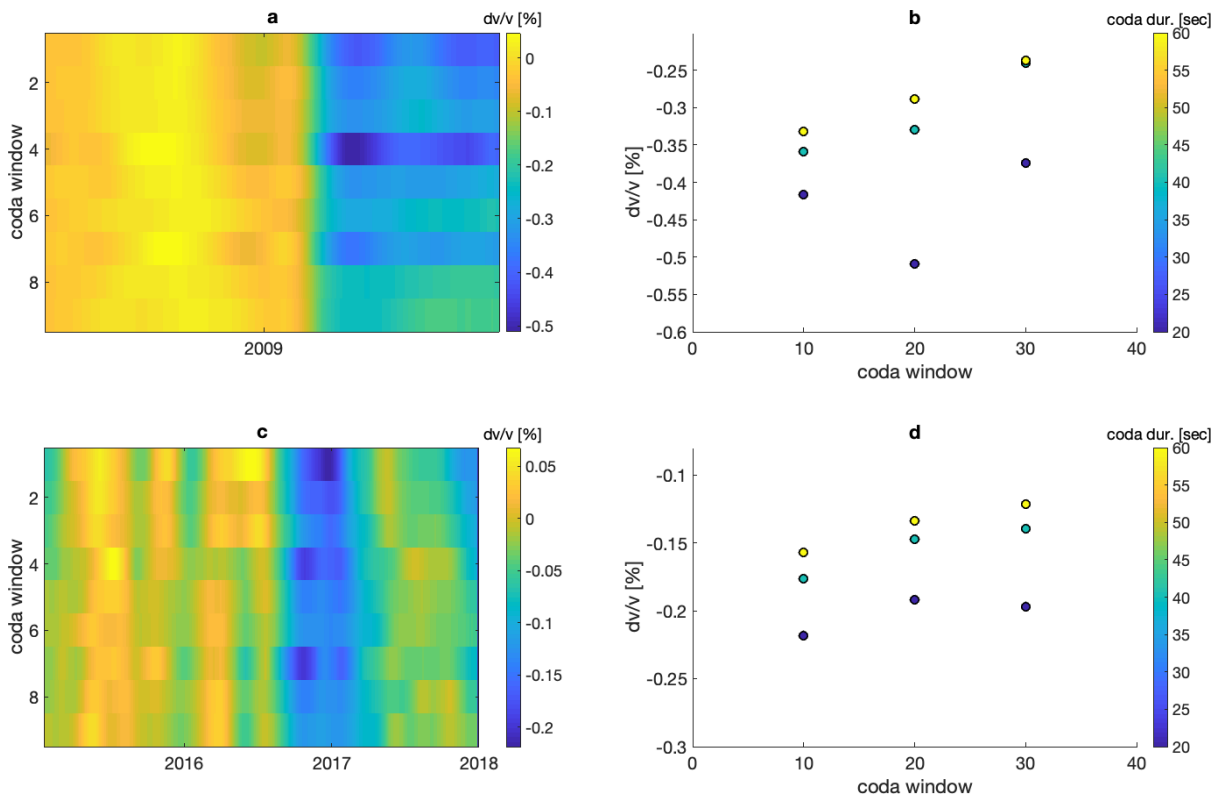
#### 4. Estimation of sensitivity to co-seismic deformation

The study region experienced three  $M > 6$  earthquakes during the period analyzed (2000-2017). The first is a magnitude  $M_w 6.1$  (Scognamiglio et al., 2010) occurring in 2009 near the city of L'Aquila with hypocentral depth at 8.3km. The station used to estimate the  $dv/v$  is located close ( $\sim 5$ km) to the epicenter and experienced a peak ground velocity of 35.8cm/s (esm.mi.ingv.it). In 2016 a series of moderate-large earthquakes (Norcia-Visso sequence) struck a region  $\sim 40$ -70km to the north of L'Aquila. The series began on the 24 of August 2016 with a magnitude 6 followed on the 30<sup>th</sup> October 2016 by a magnitude 6.5 occurring in the same region. The last two events induced a peak ground velocity  $\sim 9$ cm/s (esm.mi.ingv.it). The peak ground velocity is used to calculate the dynamic strain for the mentioned earthquakes (Taira et al, 2018, assuming  $V_s=2500$ m/s), which is respectively  $1.5e-4$  for L'Aquila event and  $4e-5$  for the 24<sup>th</sup> of August event in 2016.

In concomitance with the earthquakes, large velocity drops can be observed over the full range of the analyzed lapse times (fig. 7), similar to previous observations (Zaccarelli et al., 2011, Soldati et al., 2015). Nevertheless, we here measure the values of  $dv/v$  for each time lapse and each earthquake, and we are thus able to resolve any depth dependence response of the crust to rapid dynamic perturbation induced by large earthquakes. For each event, the velocity reduction is measured as the drop from the mean  $dv/v$  over the preceding year before the events, and the following minimum peak. For the 2016 events, our analysis window (90 days) prevents us from resolving the two drops (for the 24 of August and the 30 October events respectively). We thus consider the mean reference  $dv/v$  for the year before the first event (24<sup>th</sup> of August 2016).

397  
398  
399  
400

The co-seismic  $dv/v$  at different lapse time (Fig. 7) shows a different evolution with respect to multiyear ones (Fig. 5 and 7). For both events, we see a general reduction of  $dv/v$  as time lapse increases.



401  
402  
403  
404  
405  
406

**Figure 7:** Coseismic  $dv/v$  time series for different lapse time (Table 1) for L'Aquila 2009 event (a) and Visso-Norcia sequence 2016 (c). Coseismic velocity reduction as function of coda lapse time (Table 1) for L'Aquila 2009 event (b) and Visso-Norcia sequence 2016 (d).

## 407 Discussion

408 The analysis of the 17 years of  $dv/v$  permitted us to isolate several processes controlling  
409  $dv/v$  variations. Namely we observe velocity change due to (i) co-seismic perturbations (Fig.  
410 7), (ii) yearly perturbations likely related to variation of temperature (Fig. 4, 5) and (iii) multi-  
411 annual perturbations associated with hydrological cycles inducing dilatational strain in the  
412 crust (Fig. 4, 5, 6, Silverii et al., 2019). By estimating  $dv/v$  over different coda lapse time (Table  
413 1), we observe how the contribution from each process changes over different portions of the  
414 correlation coda (see Table 2, Fig. 5, 6, 7).

415  
416

### 416 a. Depth resolution of velocity variations

417 To interpret the results for different lapse times in term of depth, we calculated the  
418 sensitivity kernel based on the single scattering 3D radiative transfer solution considering that  
419 the measured coda waves are comprised of contributions from both body and surface waves. It  
420 is important to note that, as we have no proxy to assess the coda wave constituents, this kernel  
421 can be biased. The sensitivity to surface waves is more important for early lapse times  
422 (Obermann et al., 2013). Here we assume the value of the mean free path ( $l = 100\text{km}$  and  $10$   
423  $\text{km}$ ) and propagation velocity of coda waves  $\sim 3895$  m/s, for the equipartition state. Thus, the  
424 inferred depth sensitivity is not absolute, but we can use the kernels as an indicator of the  
425 approximate depth with lapse time. The estimated sensitivity (Fig. 2) maximum is

426 approximately  $\sim 10$ km especially for the later coda (e.g. lapse time 20 - 50s) with 50 km  
427 scattering mean free path.

428 The estimation of an absolute depth for the velocity changes will require better knowledge  
429 of the scattering properties of the medium, including its layered structure, which can play a  
430 fundamental role in trapping waves in some part of the medium (e.g. Kanu & Snieder, 2015).  
431 Here, we can only discuss the relative depth of the velocity changes observed (multiyear,  
432 seasonal, co-seismic, Fig. 5, 7) from the time lapse evolution of  $dv/v$ . For example, for multi-  
433 year deformations  $dv/v$  increases for later lapse-time (Fig. 5, 7). We thus infer the existence of  
434 a region at depth that exhibits sensitivity to long period forcing (Obermann et al., 2013, Hillers  
435 et al., 2018). The rapid decay of the B/E ratio (eq. 2, Fig. 5b), is another indication that our late  
436 coda measurements sample deeper into the crust. In fact, the thermally induced stress is  
437 expected to reduce rapidly with depth (Ben-Zion & Leary, 1986) as does the ratio (Fig. 5b).

438

439

### ***b. Origin of various velocity variation and rheology of middle crust***

440

441 We begin by discussing the strain sensitivity ( $e=[dv/v]/[de]$ ,  $de$  the dynamic strain) during  
442 the co-seismic stage. Considering the dynamic strain induced by the two events we find that  $e$   
443 is respectively  $-1e7$  and  $-1e8$  for the L'Aquila and Amatrice earthquakes respectively. These  
444 values are an order of magnitude larger than estimates in geothermal areas (Taira et al., 2018)  
445 and volcanic regions (Breguier et al., 2014), suggesting that the crustal rocks in the study  
446 region are very susceptible to dynamic deformations. Under rapid perturbations induced during  
447 large earthquakes the  $dv/v$  decreases with depth, suggesting significant nonlinear response  
448 related to damage near the surface (e.g. Obermann, 2013, 2014), or alternatively,  
449 unconsolidated granular material (e.g., Brunet et al., 2008; Johnson and Jia, 2005). For the  
450 2009 event, considering the shortest analysis window in the coda (20s, Fig. 7) a peak of  
451 maximum velocity reduction is observed, which suggests the existence of an isolated region at  
452 depth that is highly sensitive to dynamic deformations. The detailed analysis of the co-seismic  
453 response is beyond the scope of the actual work, and will be addressed in future research.

454

455 While the co-seismic rapid shaking induces large  $dv/v$  near the surface, the  $dv/v$  increases  
456 with lapse time for the long-term perturbations (Table 2, Figure 5, 6). We interpret this time  
457 lapse evolution as due to an isolated region with stronger  $dv/v$ -sensitivity to perturbations (sec.  
458 a, Obermann et al., 2013, 2014, Hillers et al., 2018). While we do not have detailed evolution  
459 of strain for the long-term  $dv/v$ , we can make a back-of-the-envelope calculation of the  
460 sensitivity, knowing that the strain at peak GPS deformation is  $\sim 1e-6$  (Silverii et al., 2019) for  
461  $\sim 1e-3$  of  $dv/v$ , which gives a  $dv/v$ -sensitivity of  $\sim 1e3$ . This latter value agrees with other  
462 estimates based on tidal- $dv/v$  responses (Yamamura et al., 2003, Takano et al. 2014). Our  
463 estimations are also in agreement with dilatant induced velocity reduction during slow slip in  
464 the lower crust (Rivet et al., 2011, Wang et al., 2019).

465

466 Laboratory studies show that nonlinear elastic modulus variation is amplitude dependent  
467 (Guyet and Johnson, 2009) as well as frequency dependent, with larger modulus changes for  
468 shorter periods for a given effective pressure (Riviere et al., 2016). Here we observe a lower  
469  $dv/v$  sensitivity ( $1e3$ ) for small quasi-static strain ( $1e-6$ ) and low frequency ( $\sim 5$ yr) in contrast  
470 to large dynamic strains ( $\sim 1e-4$ ) (lasting no more than few minutes) induced by the large  
471 earthquakes. Under low strain forcing we also observe that non-linear material slow dynamics  
472 (recovery) expressed in equation 3 is nearly zero ( $\alpha$ , Table 2). However, for short time  
473 perturbations a clear log-time recovery is observed (see for example the time after the  
474 earthquakes in figure 3a). Thus, our measures reflect general behaviors of rocks in small scale  
laboratory experiments (e.g. Riviere et al., 2016) as well as field measurements under Vibroseis  
forcing (Johnson et al., 2008) and earthquake forcing (e.g., Breguier et al., 2008; Wu et al.,  
2017; Ostrovsky et al, 2019).

475 To interpret our results, we consider the velocity variation as being controlled by crack  
476 density ( $\rho_0$ ) because it has been well documented that cracks and other damage contribute  
477 dominantly to nonlinear elastic behavior (e.g., Johnson 1998; Guyer and Johnson, 2009). The  
478 sensitivity to any stress perturbations (S) can then be written as (Silver et al., 2007):  
479

$$480 \quad e = \frac{\delta v/v}{S} = \frac{\delta v/v}{\Delta \rho_0} \frac{\Delta \rho_0}{S} \quad [4]$$

481  
482 As the crack density is expected to reduce with depth due to the lithostatic pressure (Tod,  
483 2003), sensitivity should reduce for larger lapse time (or depth) assuming fluid pressures do  
484 not vary radically. For a fixed depth dependence of strain, at shallow depth we expect larger  
485 sensitivity for larger strains, as observed during the co-seismic shaking. We again note how  
486 our results are anomalous for long-term deformation, as the sensitivity increases at depth (Table  
487 2, Figure 5, 6). The observed dichotomy (shallow response during co-seismic forcing and  
488 deeper response during long-term forcing) is similar to what has been observed in Wenchuan  
489 area by Obermann et al., (2014).

490 The cause of velocity variation at late lapse time may be due to meteorological water  
491 circulation in the crust. However, in this case we would expect velocity changes also at shallow  
492 depth (early lapse time). Thus, alternative mechanism(s) inducing changes may exist. A  
493 possibility is that forcing induced by water table variation, rather than water itself, is  
494 responsible for velocity changes, with the loading (unloading) inducing significantly increment  
495 (reduction) of the pore pressure and controlling the drop (increment) of velocity (Froment et  
496 al., 2013, Obermann et al., 2014). This mechanism has also been observed and modeled in the  
497 Irpinia region (D'Agostino et al., 2018).

498 The presence of pressurized fluids at depth a range 5-10km has been suggested by several  
499 researchers for the region of L'Aquila, from analysis of earthquake source properties  
500 (Tarekawa et al., 2010, Malagnini et al., 2012) or from Vp/Vs ratio (Di Luccio et al, 2012).  
501 Other studies suggest an extensive dilatancy anisotropy in the central Apennines, related to  
502 pervasive fluid-filled cracks oriented parallel to the Apennines chain (Pastori et al., 2016).  
503 Furthermore, a significant presence of a damage zone comprised of near-fault cracks (up to  
504 ~1km from the fault) are observed in the carbonate rocks near the region of L'Aquila (Agosta  
505 & Aydin, 2006).

506 Putting together our results with the other geophysical information, suggests the existence  
507 of a depth-isolated and long-lived (at least 9 years), intensely cracked and fluid rich, damaged  
508 region in the study area. At this depth, the strong sensitivity (equation 3 and 4) is related to the  
509 presence of fluids, reducing the effective pressure, thus favoring high crack density (Hamiel et  
510 al., 2006) and making the material more susceptible to dynamic or quasi-static forcing.

511 Mid-crustal damage zones have been also observed in California by analysis of seismic  
512 catalogs (Ben-Zion & Zaliapin, 2019). Highlighting the existence of such a damage zone is  
513 fundamental as damage plays a key role in the evolution of the seismic cycle and earthquake  
514 nucleation (Lyakhovskiy et al., 2001, Renard et al., 2018) and controls the amount of strain  
515 released in a brittle manner during the seismic cycle (Hamiel et al., 2006). For example,  
516 numerical simulations show that nucleation and growth of large earthquakes is only possible  
517 with the existence of a, at least modestly, damaged region (Lyakhovskiy et al., 2001). Indeed,  
518 Ben-Zion & Zaliapin (2019) highlighted significant damage volumes active prior to several  
519 significant earthquakes in California. In a similar manner, intense seismic activity was  
520 observed, concentrated near the nucleation depth of L'Aquila earthquake, in the last year  
521 preceding the mainshock (e.g. Valoroso et al., 2013). Whereas seismicity solely provides a  
522 volume of damage (Ben-Zion & Zaliapin, 2019), we quantitatively estimate rheological  
523 parameters (e.g. sensitivity) of rocks at depth in a region of important seismic hazard.

524 The presence of a highly fractured rocks has implication for earthquake nucleation models.  
 525 The influence of damage on a critical phase transition model has been described by Renard and  
 526 others (Renard et al., 2018). In this model, cracks become more interconnected as a large event  
 527 is approaching, and progressively merge into a single primary fracture (the main shock). Close  
 528 to the main rupture significant precursory earthquakes must occur in the damage zone (Renard  
 529 et al., 2018), similarly to what is observed in the year preceding the L'Aquila earthquake in  
 530 2009 (e.g. Valoroso et al., 2013).

531 We finally note (fig. 3a) how the seasonal cycle seems to disappear after the 2009 L'Aquila  
 532 earthquake. Given that rain cycle remains significant after 2009, this behavior seems to suggest  
 533 less sensitivity of the medium after the earthquake. However, there might exists a possible  
 534 interplay between the long and slow post-seismic recovery and multiyear cycle, which will be  
 535 studied in future works. Further, fluid pressures could play a key role—decreased pressures  
 536 allow cracks to close and elastic non-linearity to decrease. This point needs further work.

537  
 538 **Table 2: Summary of derived parameters**

Window number	1-year cycle (eq. 2)	5 years cycle (eq. 2)	$\alpha$ (eq. 3)	$\beta$ (eq. 3)	L'Aquila $dv/v$ PGV=35.8cm/s Strain=1.5e-4	Amatrice $dv/v$ PGV=9cm/s Strain=4e-5
1	<b>0.036</b>	0.01	0.006	1.65	-0.39	<b>-0.18</b>
2	0.02	0.02	0.005	-1.22	-0.34	-0.1543
3	0.02	0.01	0.004	-2.22	-0.31	-0.12
4	0.02	<b>0.04</b>	<b>0.008</b>	<b>-11.56</b>	<b>-0.49</b>	-0.1545
5	0.01	0.03	0.005	-7.83	-0.32	-0.11
6	0.00	0.02	0.004	-6.82	-0.28	-0.0917
7	0.01	<b>0.04</b>	<b>0.008</b>	-8.79	-0.36	-0.15
8	0.00	0.03	0.005	-8.76	-0.23	-0.1548
9	0.00	0.02	0.004	-6.36	-0.23	-0.08

542

550  
 551 **a. Towards monitoring with seasonal loading**

552 We showed that seasonal and multiyear components dominate the  $dv/v$  time series in the  
 553 inter-seismic period (figs. 4, 5). These cycles are likely to mask smaller tectonic signals (e.g.  
 554 fault weakening during earthquake preparation or transient tectonic deformations among).  
 555 Indeed, systematic efforts have been applied to characterize the cyclic variations by modeling  
 556 them (Wang et al. 2017) or by estimating the repeating patterns over several cycles and use  
 557 their average as correction to isolate tectonic signals (Hillers et al., 2018).

558 Knowing the physical processes responsible for multiannual  $dv/v$  evolution (Silverii et al,  
 559 2019), we assessed the lapse time dependent response of the medium to these cycles of  
 560 dilatational strain, thus turning a nuisance into an opportunity to study the crust in a region of  
 561 significant seismic hazard. This approach is similar to the studies of tidal induced  $dv/v$  (Takano  
 562 et al., 2014, Hillers et al., 2015b), but we here assess longer cycles, and sample deeper regions  
 563 in the crust near a main active fault.

564 Our lapse time  $dv/v$  analysis bears similarities to laboratory dynamic nonlinear studies  
 565 applied to resolve the spatial extent of damaged regions in solids (e.g., Johnson, 1998; Ulrich  
 566 et al., 2007; Guyer and Johnson, 2009; Ostrovsky and Johnson, 2001; Hauptert et al., 2014). As  
 567 in these studies we observe a maximum response to deformation of the medium ( $\beta$ , eq. 3) in  
 568 the damaged zone. Strain concentration can also produce highly localized increases in  
 569 nonlinear response (Lott et al., 2016) especially at crack tips (e.g., Ulrich 2006), and thus time  
 570 lapse monitoring could be used to reveal zones of anomalous strain accumulation.

571 The extension of our analysis to other regions, instrumented with dense geodetic networks  
 572 and or application of InSAR allowing the accurate estimate of time-dependent strain, will help  
 573 to better assess the physical properties of rocks at depth (e.g. assessing conditioning, slow



574 dynamics and hysteresis [Guyet and Johnson, 2009; TenCate et al., 2000]). Potential regions  
575 for new studies include New Madrid seismic zone (Craig et al., 2017) or the Himalayan region  
576 (Bettinelli et al., 2008, Bollinger et al., 2007), or Irpinia (D'Agostino et al., 2018). These  
577 regions are characterized by significant seismic risk, prominent seasonal and multiannual  
578 perturbations, and excellent seismological and geodetic instrumentation.

579

## 580 **5. Conclusions**

581 The precise analysis of time lapse velocity variations for 17 years of data in the region of  
582 L'Aquila permitted us to unravel the complex behavior of multiple processes controlling the  
583  $dv/v$  evolution, over a wide range of temporal and spatial scales. The comparison of  $dv/v$  with  
584 independent measurements (e.g. dynamic strain induced by earthquakes, quasi-static strain due  
585 to hydrological cycles) permitted us to characterize the rheological response of seismogenic  
586 rocks to various level of strain at various depths. The time-lapse analysis allowed us to resolve  
587 a dichotomy in the crustal response, with significant near surface damage due to rapid strain  
588 induced by large earthquakes and deeper strain sensitivity due to long period (5yrs) and small  
589 strain perturbations in an inferred damage zone containing high fluid pressures, where the  
590 mainshock earthquake nucleates.

591 We showed that when the physical processes responsible for seasonal or multiyear cycles  
592 can be quantitatively characterized (e.g. Silverii et al., 2019), they can be exploited to evaluate  
593 the rheological properties of rocks in the crust. This work extends previous approaches based  
594 on tidal strain- $dv/v$  evaluation, which are primarily sensitive to the shallowest part of the crust  
595 ( $< \sim 1$ km, e.g. Takano et al. 2014). Furthermore, our analysis made it possible to turn  
596 hydrologically-induced cycles of  $dv/v$ , usually seen as a nuisance as they can mask tectonic  
597 events, into an opportunity to reveal the rheology of crustal rocks down to the seismogenic  
598 depth. Extending this work to other seismic active region, affected by significant weather-  
599 related cycles (Bettinelli et al., 2008, Bollinger et al., 2007, D'Agostino et al., 2018, Craig et  
600 al., 2017) will reveal new information about the physical properties of near fault rocks.

601

## 602 **Acknowledgements**

603 This research received funding from the European Research Council (ERC) under the  
604 European Union Horizon 2020 Research and Innovation Programme (grant agreements,  
605 802777-MONIFaults). PAJ was supported by the US DOE Office of Science, Chemical  
606 Sciences, Geosciences, and Biosciences. QW was supported by the ERCproject 742335-F-  
607 IMAGE. The article benefited greatly from discussions with Yehuda Ben-Zion, William Frank,  
608 Michele Fondriest, Ivan Callegari, Michel Campillo, Martin Lott and Leonard Seydoux. The  
609 rain and temperature data have were graciously provided by the Ufficio Idrografico  
610 Mareografico of the Abruzzo region. The seismic data are available at Istituto Nazionale di  
611 Geofisica e Vulcanologia (<http://iside.rm.ingv.it/instruments>) and at Incorporated Research  
612 Institution for Seismology (<https://www.iris.edu/hq/>).

613

614

## 615 **Bibliography**

616

617

618 *Agosta, Fabrizio, and Atilla Aydin. "Architecture and deformation mechanism of a basin-*  
619 *bounding normal fault in Mesozoic platform carbonates, central Italy." *Journal of Structural**

620 *Geology* 28.8 (2006): 1445-1467.

621

622 *Avallone, Antonio, et al. "The RING network: improvement of a GPS velocity field in the*

623 *central Mediterranean." *Annals of Geophysics* 53.2 (2010): 39-54.*

624  
625 *Ben-Zion, Yehuda. "Collective behavior of earthquakes and faults: Continuum-discrete*  
626 *transitions, progressive evolutionary changes, and different dynamic regimes." Reviews of*  
627 *Geophysics 46.4 (2008).*  
628  
629 *Ben-Zion, Yehuda, and Peter Leary. "Thermoelastic strain in a half-space covered by*  
630 *unconsolidated material." Bulletin of the Seismological Society of America 76.5 (1986): 1447-*  
631 *1460.*  
632  
633 *Ben-Zion, Yehuda, and Ilya Zaliapin. "Spatial variations of rock damage production by*  
634 *earthquakes in southern California." Earth and Planetary Science Letters 512 (2019): 184-*  
635 *193.*  
636  
637 *Bettinelli, Pierre, et al. "Seasonal variations of seismicity and geodetic strain in the Himalaya*  
638 *induced by surface hydrology." Earth and Planetary Science Letters 266.3-4 (2008): 332-344.*  
639  
640 *Bollinger, L., et al. "Seasonal modulation of seismicity in the Himalaya of Nepal." Geophysical*  
641 *Research Letters 34.8 (2007).*  
642  
643 *Brenguier, F., et al. "Mapping pressurized volcanic fluids from induced crustal seismic velocity*  
644 *drops." Science 345.6192 (2014): 80-82.*  
645  
646 *Brenguier, Florent, et al. "Postseismic relaxation along the San Andreas fault at Parkfield*  
647 *from continuous seismological observations." science 321.5895 (2008): 1478-1481.*  
648  
649 *Brunet, T., X. Jia and P. Johnson, Transitional, elastic-nonlinear behaviour in dense granular*  
650 *media, Geophys. Res. Lett. 35, L19308-L19311 doi:10.1029/2008GL035264 (2008).*  
651  
652 *Chiaraluce, L., et al. "The 2009 L'Aquila (Central Italy) Seismic Sequence." Bollettino di*  
653 *Geofisica Teorica e Applicata. (2010).*  
654  
655  
656 *Chiaraluce, L., et al. "The anatomy of the 2009 L'Aquila normal fault system (central Italy)*  
657 *imaged by high resolution foreshock and aftershock locations." Journal of Geophysical*  
658 *Research: Solid Earth 116.B12 (2011).*  
659  
660 *Craig, Timothy J., Kristel Chanard, and Eric Calais. "Hydrologically-driven crustal stresses*  
661 *and seismicity in the New Madrid Seismic Zone." Nature communications 8.1 (2017): 2143.*  
662  
663 *Chiaraluce, Lauro, et al. "The 2016 central Italy seismic sequence: A first look at the*  
664 *mainshocks, aftershocks, and source models." Seismological Research Letters 88.3 (2017):*  
665 *757-771.*  
666  
667 *Chiaraluce, L. "Unravelling the complexity of Apenninic extensional fault systems: a review of*  
668 *the 2009 L'Aquila earthquake (Central Apennines, Italy)." Journal of Structural Geology 42*  
669 *(2012): 2-18.*  
670  
671 *D'Agostino, N. "Complete seismic release of tectonic strain and earthquake recurrence in the*  
672 *Apennines (Italy)." Geophysical Research Letters 41.4 (2014): 1155-1162.*  
673

674 D'Agostino, Nicola, et al. "Crustal deformation and seismicity modulated by groundwater  
675 recharge of karst aquifers." *Geophysical Research Letters* 45.22 (2018): 12-253.  
676

677 Delorey, Andrew A., Nicholas J. van der Elst, and Paul A. Johnson. "Tidal triggering of  
678 earthquakes suggests poroelastic behavior on the San Andreas Fault." *Earth and Planetary  
679 Science Letters* 460 (2017): 164-170.  
680

681 Di Luccio, F., et al. "Normal faults and thrusts reactivated by deep fluids: The 6 April 2009  
682 Mw 6.3 L'Aquila earthquake, central Italy." *Journal of Geophysical Research: Solid  
683 Earth* 115.B6 (2010).  
684

685 Froment, B., et al. "Deformation at depth associated with the 12 May 2008 Mw 7.9 Wenchuan  
686 earthquake from seismic ambient noise monitoring." *Geophysical Research Letters* 40.1  
687 (2013): 78-82.  
688

689 Guyer, Robert A., and Paul A. Johnson. "Nonlinear mesoscopic elasticity: Evidence for a new  
690 class of materials." *Physics today* 52 (1999): 30-36.  
691

692 Guyer, Robert A., and Paul A. Johnson. *Nonlinear mesoscopic elasticity: the complex  
693 behaviour of rocks, soil, concrete.* John Wiley & Sons, 2009.  
694

695 Hamiel, Yariv, et al. "Stable and unstable damage evolution in rocks with implications to  
696 fracturing of granite." *Geophysical Journal International* 167.2 (2006): 1005-1016.  
697

698 Herrmann, R. B. (2013). *Computer programs in seismology: An evolving tool for instruction  
699 and research.* *Seismological Research Letters*,  
700 84(6), 1081–1088. <https://doi.org/10.1785/0220110096>  
701  
702

703 Hauptert, Sylvain, et al. "Optimized dynamic acousto-elasticity applied to fatigue damage and  
704 stress corrosion cracking." *Journal of Nondestructive Evaluation* 33.2 (2014): 226-238.  
705

706 Hillers, G., et al. "Seasonal variations of seismic velocities in the San Jacinto fault area  
707 observed with ambient seismic noise." *Geophysical Journal International* 202.2 (2015a): 920-  
708 932.  
709

710 Hillers, G., et al. "In situ observations of velocity changes in response to tidal deformation  
711 from analysis of the high-frequency ambient wavefield." *Journal of Geophysical Research:  
712 Solid Earth* 120.1 (2015b): 210-225.  
713

714 Hillers, Gregor, et al. "Transient change of seismic velocities in the San Jacinto fault region  
715 following the 2010 M7. 2 El Mayor-Cucapah earthquake observed with ambient noise  
716 monitoring." *EGU General Assembly Conference Abstracts. Vol. 20. 2018.*  
717

718 Johnson, P. A. and X. Jia, *Nonlinear dynamics, granular media and dynamic earthquake  
719 triggering, Nature*, 473 871-874 (2005)  
720

721 Johnson, P., Robert Guyer, and L. Ostrovsky. *A nonlinear mesoscopic elastic class of  
722 materials.* No. LA-UR-99-4733. Los Alamos National Lab., NM (US), 1999.  
723

724 Johnson, Paul A. "The new wave in acoustic testing." *Materials World* (1999): 544-546.  
725

726 Johnson, Paul A., et al. "Inducing in situ, nonlinear soil response applying an active  
727 source." *Journal of Geophysical Research: Solid Earth* 114.B5 (2009).  
728

729 Kanu, Chinaemerem, and Roel Snieder. "Numerical computation of the sensitivity kernel for  
730 monitoring weak changes with multiply scattered acoustic waves." *Geophysical Supplements  
731 to the Monthly Notices of the Royal Astronomical Society* 203.3 (2015): 1923-1936.  
732

733 Lacombe, Céline, et al. "Separation of intrinsic absorption and scattering attenuation from  
734 Lg coda decay in central France using acoustic radiative transfer theory." *Geophysical  
735 Journal International* 154.2 (2003): 417-425.  
736

737 L.D. Landau & E.M. Lifshitz *Theory of Elasticity (Volume 7 of A Course of Theoretical  
738 Physics)* Pergamon Press 1970  
739

740 Lobkis, O. I., and R. L. Weaver (2003), Coda-wave interferometry in finite solids: Recovery of  
741 P-to-S conversion rates in an elastodynamic billiard, *Phys. Rev. Lett.*, 90(25), 254302,  
742 doi:10.1103/PhysRevLett.90.254302.  
743

744 Lott, Martin, et al. "From local to global measurements of nonclassical nonlinear elastic  
745 effects in geomaterials." *The Journal of the Acoustical Society of America* 140.3 (2016):  
746 EL231-EL235.

747 Lott, Martin, et al. "Three-dimensional modeling and numerical predictions of multimodal  
748 nonlinear behavior in damaged concrete blocks." *The Journal of the Acoustical Society of  
749 America* 144.3 (2018): 1154-1159.

750 Lyakhovskiy, V., Ben-Zion, Y., Agnon, A., 2001. Earthquake cycle, fault zones, and seismicity  
751 patterns in a rheologically layered lithosphere. *J. Geophys. Res.* 106, 4103–4120.

752 Malagnini, Luca, et al. "Control of pore fluid pressure diffusion on fault failure mode: Insights  
753 from the 2009 L'Aquila seismic sequence." *Journal of Geophysical Research: Solid  
754 Earth* 117.B5 (2012).  
755

756 Margerin, Ludovic, Michel Campillo, and Bart Van Tiggelen. "Monte Carlo simulation of  
757 multiple scattering of elastic waves." *Journal of Geophysical Research: Solid Earth* 105.B4  
758 (2000): 7873-7892.  
759

760 McCall, K. R., and R. A. Guyer. *Hysteresis and nonlinear elasticity in rocks*. No. LA-UR-93-  
761 4143; CONF-9308167-5. Los Alamos National Lab., NM (United States), 1993.  
762

763 Obermann, Anne, et al. "Depth sensitivity of seismic coda waves to velocity perturbations in  
764 an elastic heterogeneous medium." *Geophysical Journal International* 194.1 (2013): 372-382.  
765

766 Obermann, Anne, et al. "Seismic noise correlations to image structural and mechanical  
767 changes associated with the Mw 7.9 2008 Wenchuan earthquake." *Journal of Geophysical  
768 Research: Solid Earth* 119.4 (2014): 3155-3168.  
769

770 Ostrovsky, L. A., and P. A. Johnson. "Dynamic nonlinear elasticity in geo materials." *Rivista*  
771 *del Nuovo Cimento della Societa Italiana di Fisica* 24.7 (2001): 1-46.  
772

773 Ostrovsky, Lev, et al. "Long-Time Relaxation Induced by Dynamic Forcing in  
774 Geomaterials." *Journal of Geophysical Research: Solid Earth* (2019).  
775

776 Pacheco, Carlos, and Roel Snieder. "Time-lapse travel time change of multiply scattered  
777 acoustic waves." *The Journal of the Acoustical Society of America* 118.3 (2005): 1300-1310.  
778

779 Paasschens, J. C. J. "Solution of the time-dependent Boltzmann equation." *Physical Review*  
780 *E* 56.1 (1997): 1135.  
781

782 Pastori, Marina, Paola Baccheschi, and Lucia Margheriti. "Shear wave splitting evidence and  
783 relations with stress field and major faults from the "Amatrice-Visso-Norcia Seismic  
784 Sequence". " *Tectonics* (2019).  
785

786 Planès, Thomas, et al. "Decorrelation and phase-shift of coda waves induced by local changes:  
787 multiple scattering approach and numerical validation." *Waves in Random and Complex*  
788 *Media* 24.2 (2014): 99-125.  
789

790 Poli, P., et al. "Noise directivity and group velocity tomography in a region with small velocity  
791 contrasts: the northern Baltic shield." *Geophysical Journal International* 192.1 (2012): 413-  
792 424.  
793

794 Poupinet, G., W. Ellsworth, and J. Frechet (1984), *Monitoring velocity variations in the crust*  
795 *using earthquake doublets: An application to the Calaveras Fault, California, J. Geophys.*  
796 *Res.*, 89(B7), 5719–5731.

797 Renard, F., Weiss, J., Mathiesen, J., Ben Zion, Y., Kandula, N., Cordonnier, B., 2018. *Critical*  
798 *evolution of damage towards system-size failure in crystalline rock. J. Geophys. Res.* 123,  
799 1969–1986. <https://doi.org/10.1002/2017JB014964>.

800 Renaud, Guillaume, Samuel Callé, and Marielle Defontaine. "Remote dynamic acoustoelastic  
801 testing: Elastic and dissipative acoustic nonlinearities measured under hydrostatic tension and  
802 compression." *Applied Physics Letters* 94.1 (2009): 011905.  
803

804 Renaud, G., P-Y. Le Bas, and P. A. Johnson. "Revealing highly complex elastic nonlinear  
805 (anelastic) behavior of Earth materials applying a new probe: Dynamic acoustoelastic  
806 testing." *Journal of Geophysical Research: Solid Earth* 117.B6 (2012).  
807

808 Richter, Tom, et al. "Comprehensive observation and modeling of earthquake and  
809 temperature-related seismic velocity changes in northern Chile with passive image  
810 interferometry." *Journal of Geophysical Research: Solid Earth* 119.6 (2014): 4747-4765.  
811

812 Rivet, Diane, et al. "Seismic evidence of nonlinear crustal deformation during a large slow slip  
813 event in Mexico." *Geophysical Research Letters* 38.8 (2011).  
814

815 Rivière, J., L. Pimienta, M. Scuderi, T. Candela, P. Shokouhi, J. Fortin, A. Schubnel, C. Marone,  
816 and P. A. Johnson (2016), *Frequency, pressure, and strain dependence of nonlinear elasticity*  
817 *in Berea Sandstone, Geophys. Res. Lett.*, 43, 3226–3236, doi:10.1002/2016GL068061.

818 *Rivière, Jacques & Shokouhi, Parisa & Guyer, Robert & Johnson, Paul. (2015). A set of*  
819 *measures for the systematic classification of the nonlinear elastic behavior of disparate rocks.*  
820 *Journal of Geophysical Research: Solid Earth. 120. 10.1002/2014JB011718.*  
821

822 *Sabra, Karim G., et al. "Extracting time-domain Green's function estimates from ambient*  
823 *seismic noise." Geophysical Research Letters 32.3 (2005).*  
824

825 *Scognamiglio, L., Tinti, E., Quintiliani, M. (2006). Time Domain Moment Tensor [Data set]. Istituto*  
826 *Nazionale di Geofisica e Vulcanologia (INGV). <https://doi.org/10.13127/TDMT>*  
827

828 *Scognamiglio, Laura, et al. "Fast determination of moment tensors and rupture history: What*  
829 *has been learned from the 6 April 2009 L'Aquila earthquake sequence." Seismological*  
830 *Research Letters 81.6 (2010): 892-906.*  
831

832 *Sens-Schönfelder, Christoph, Roel Snieder, and Xun Li. "A model for nonlinear elasticity in*  
833 *rocks based on friction of internal interfaces and contact aging." Geophysical Journal*  
834 *International 216.1 (2018): 319-331.*  
835

836 *Soldati, Gaia, et al. "Monitoring of crustal seismic velocity variations in the L'Aquila fault*  
837 *zone inferred from noise cross-correlation." Geophysical Journal International 202.1 (2015):*  
838 *604-611.*  
839

840 *Shapiro, Nikolai M., and Michel Campillo. "Emergence of broadband Rayleigh waves from*  
841 *correlations of the ambient seismic noise." Geophysical Research Letters 31.7 (2004).*  
842

843 *Silver, Paul G., et al. "Active source monitoring of cross-well seismic travel time for stress-*  
844 *induced changes." Bulletin of the Seismological Society of America 97.1B (2007): 281-293.*  
845

846 *Silverii, Francesca, et al. "Transient deformation of karst aquifers due to seasonal and*  
847 *multiyear groundwater variations observed by GPS in southern Apennines (Italy)." Journal of*  
848 *Geophysical Research: Solid Earth 121.11 (2016): 8315-8337.*  
849

850 *Silverii, Francesca, et al. "Transient crustal deformation from karst aquifers hydrology in the*  
851 *Apennines (Italy)." Earth and Planetary Science Letters 506 (2019): 23-37.*  
852

853 *TenCate, J.A., E. Smith, and R.t A. Guyer, Universal Slow Dynamics in Granular Solids. Phys.*  
854 *Rev. Lett. 85, 1020 (2000)*  
855

856 *Van Den Abeele, Koen & Visscher, Joëlle. (2000). Damage Assessment in reinforced concrete*  
857 *using spectral and temporal nonlinear vibration techniques. Cement and Concrete Research.*  
858 *30. 1453-1464. 10.1016/S0008-8846(00)00329-X.*  
859

860 *van der Elst, Nicholas J., et al. "Fortnightly modulation of San Andreas tremor and low-*  
861 *frequency earthquakes." Proceedings of the National Academy of Sciences 113.31 (2016):*  
862 *8601-8605.*  
863

864 *Valoroso, L., et al. "Radiography of a normal fault system by 64,000 high-precision earthquake*  
865 *locations: The 2009 L'Aquila (central Italy) case study." Journal of Geophysical Research:*  
866 *Solid Earth 118.3 (2013): 1156-1176.*  
867



868 Weaver, Richard L. "On diffuse waves in solid media." *The Journal of the Acoustical Society*  
869 *of America* 71.6 (1982): 1608-1609.

870

871 Yamamura, Keiko, et al. "Long-term observation of in situ seismic velocity and  
872 attenuation." *Journal of Geophysical Research: Solid Earth* 108.B6 (2003).

873

874 Taira, Taka'aki, et al. "Monitoring reservoir response to earthquakes and fluid extraction,  
875 Salton Sea geothermal field, California." *Science Advances* 4.1 (2018): e1701536.

876

877 Takano, Tomoya, et al. "Seismic velocity changes caused by the Earth tide: Ambient noise  
878 correlation analyses of small-array data." *Geophysical Research Letters* 41.17 (2014): 6131-  
879 6136.

880

881 Terakawa, Toshiko, et al. "High-pressure fluid at hypocentral depths in the L'Aquila region  
882 inferred from earthquake focal mechanisms." *Geology* 38.11 (2010): 995-998.

883

884 Tod, S. R. "Bed-limited cracks in effective medium theory." *Geophysical Journal*  
885 *International* 152.2 (2003): 344-352.

886

887 Ulrich, T. J., P. A. Johnson, and R. A. Guyer, *Interaction Dynamics of Elastic Waves with a*  
888 *Complex Nonlinear Scatterer through the Use of a Time Reversal Mirror*, *Phys. Rev. Lett.* 98,  
889 104301 (2007).

890

891 Wang, Qing-Yu, et al. "Seasonal crustal seismic velocity changes throughout Japan." *Journal*  
892 *of Geophysical Research: Solid Earth* 122.10 (2017): 7987-8002.

893

894 Wang, Qing-Yu, et al. "Evidence of changes of seismic properties in the entire crust beneath  
895 Japan after the Mw 9.0, 2011 Tohoku-oki earthquake." *Journal of Geophysical Research:*  
896 *Solid Earth* (2019).

897

898 Wu, Chunquan, et al. "Constraining depth range of S wave velocity decrease after large  
899 earthquakes near Parkfield, California." *Geophysical Research Letters* 43.12 (2016): 6129-  
900 6136.

901

902 Zaccarelli, Lucia, et al. "Variations of crustal elastic properties during the 2009 L'Aquila  
903 earthquake inferred from cross-correlations of ambient seismic noise." *Geophysical Research*  
904 *Letters* 38.24 (2011).

905

906

907

908

909

910